Report

Current Biology

Theta, but Not Gamma Oscillations in Area V4 Depend on Input from Primary Visual Cortex

Highlights

- Visual stimulation elicits theta and gamma oscillations in V1 and V4
- Theta and gamma oscillations interact in time
- Although lesion of V1 eliminates V4 theta oscillations, gamma oscillations survive
- Gamma oscillations still contain stimulus information but emerge delayed without V1

Authors

Ricardo Kienitz, Michele A. Cox, Kacie Dougherty, ..., David A. Leopold, Alexander Maier, Michael C. Schmid

Correspondence

michael.schmid@unifr.ch (M.C.S.), ricardo.kienitz@esi-frankfurt.de (R.K.)

In Brief

Kienitz et al. show that, upon visual stimulation, V1 and V4 show theta and gamma oscillations, which interacted in terms of phase-to-amplitude coupling. Lesion of V1, the major input source to V4, eliminated V4 theta oscillations. In contrast, V4 gamma oscillations were less affected and still contained stimulus information but emerged delayed (>100 ms).

Kienitz et al., 2021, Current Biology *31*, 1–8
February 8, 2021
https://doi.org/10.1016/j.cub.2020.10.091

CellPress

Please cite this article in press as: Kienitz et al., Theta, but Not Gamma Oscillations in Area V4 Depend on Input from Primary Visual Cortex, Current Biology (2020), https://doi.org/10.1016/j.cub.2020.10.091

Current Biology

CellPress
OPEN ACCESS

Report

Theta, but Not Gamma Oscillations in Area V4 Depend on Input from Primary Visual Cortex

Ricardo Kienitz,[1,2,3,10,*] Michele A. Cox,[4,5] Kacie Dougherty,[4,6] Richard C. Saunders,[7] Joscha T. Schmiedt,[1] David A. Leopold,[7,8] Alexander Maier,[4] and Michael C. Schmid[2,9,*]

[1]Ernst Strüngmann Institute (ESI) for Neuroscience in Cooperation with Max Planck Society, Deutschordenstraße 46, 60528 Frankfurt am Main, Germany

[2]Biosciences Institute, Faculty of Medical Sciences, Newcastle University, Newcastle upon Tyne NE2 4HH, UK

[3]Epilepsy Center Frankfurt Rhine-Main, Center of Neurology and Neurosurgery, Goethe University, Schleusenweg 2-16, 60528 Frankfurt am Main, Germany

[4]Department of Psychology, Vanderbilt University, 111 21st Avenue South, 301 Wilson Hall, Nashville, TN 37240, USA

[5]Center for Visual Science, University of Rochester, Meliora Hall, Rochester, NY 14627, USA

[6]Princeton Neuroscience Institute, Princeton University, Washington Road, Princeton, NJ 08544, USA

[7]Laboratory of Neuropsychology, NIMH, Convent Drive 49, Bethesda, MD 20892, USA

[8]Neurophysiology Imaging Facility, NIMH, NINDS and NEI, 49 Convent Drive, Bethesda, MD 20892, USA

[9]Department of Neuroscience and Movement Science, Faculty of Science and Medicine, University of Fribourg, Chemin du Musée 5, 1700 Fribourg, Switzerland

[10]Lead Contact

*Correspondence: ricardo.kienitz@esi-frankfurt.de (R.K.), michael.schmid@unifr.ch (M.C.S.)

https://doi.org/10.1016/j.cub.2020.10.091

SUMMARY

Theta (3–9 Hz) and gamma (30–100 Hz) oscillations have been observed at different levels along the hierarchy of cortical areas and across a wide set of cognitive tasks. In the visual system, the emergence of both rhythms in primary visual cortex (V1) and mid-level cortical areas V4 has been linked with variations in perceptual reaction times.[1–5] Based on analytical methods to infer causality in neural activation patterns, it was concluded that gamma and theta oscillations might both reflect feedforward sensory processing from V1 to V4.[6–10] Here, we report on experiments in macaque monkeys in which we experimentally assessed the presence of both oscillations in the neural activity recorded from multi-electrode arrays in V1 and V4 before and after a permanent V1 lesion. With intact cortex, theta and gamma oscillations could be reliably elicited in V1 and V4 when monkeys viewed a visual contour illusion and showed phase-to-amplitude coupling. Laminar analysis in V1 revealed that both theta and gamma oscillations occurred primarily in the supragranular layers, the cortical output compartment of V1. However, there was a clear dissociation between the two rhythms in V4 that became apparent when the major feedforward input to V4 was removed by lesioning V1: although V1 lesioning eliminated V4 theta, it had little effect on V4 gamma power except for delaying its emergence by >100 ms. These findings suggest that theta is more tightly associated with feedforward processing than gamma and pose limits on the proposed role of gamma as a feedforward mechanism.

RESULTS

Visual Stimulation Elicits Theta and Gamma Activity in V1 and V4

To assess theta and gamma oscillations across two different levels of the cortical hierarchy, we recorded multi-unit activity (MUA) and local field potential (LFP) in visual areas primary visual cortex (V1) and V4 in monkeys that passively viewed a visual contour (“Kanizsa”) illusion and its non-illusory control (Figure 1A). This visual stimulation elicited robust increases in MUA both in V1 and V4, whereas stimulus-specific effects across channels were only seen in V4 (Figures 1B, 1C, and S1A; Table S1; see also Figures 4E and 4F, left panels, left wings). In addition to this increase in firing rates after stimulus onset, spectral analyses of MUA responses focusing on the sustained response period after stimulus onset (0.3–1 s) revealed significant theta oscillations both in V1 and V4 and gamma oscillations in V1 (Figures 1B, 1C, and S1A; see Table S2 for detailed statistics). In contrast to the non-rhythmic MUA in V1, both the theta and gamma modulation of V1 MUA showed significantly stronger increases for the illusion compared to the control (Figure 1B; Table S2). Similarly, V4 exhibited strong theta oscillations associated with the Kanizsa illusion (Figure 1C; see also Figure 4E, right panel, left wing, and 4F, right panel, left wing; Table S2).

Analysis of V1 LFP revealed that all channels showed theta and gamma power increases following visual stimulation. However, in contrast to the rhythmic MUA, these power changes were not significantly modulated by the presence of the illusion (Figures 1D and S1B; Table S3; theta: $p = 0.99$; gamma: $p = 0.97$; $n = 61$; Wilcoxon rank sum test). V4 LFP exhibited similar theta oscillations as V4 MUA. Yet, compared to V4 MUA, it

Please cite this article in press as: Kienitz et al., Theta, but Not Gamma Oscillations in Area V4 Depend on Input from Primary Visual Cortex, Current Biology (2020), https://doi.org/10.1016/j.cub.2020.10.091

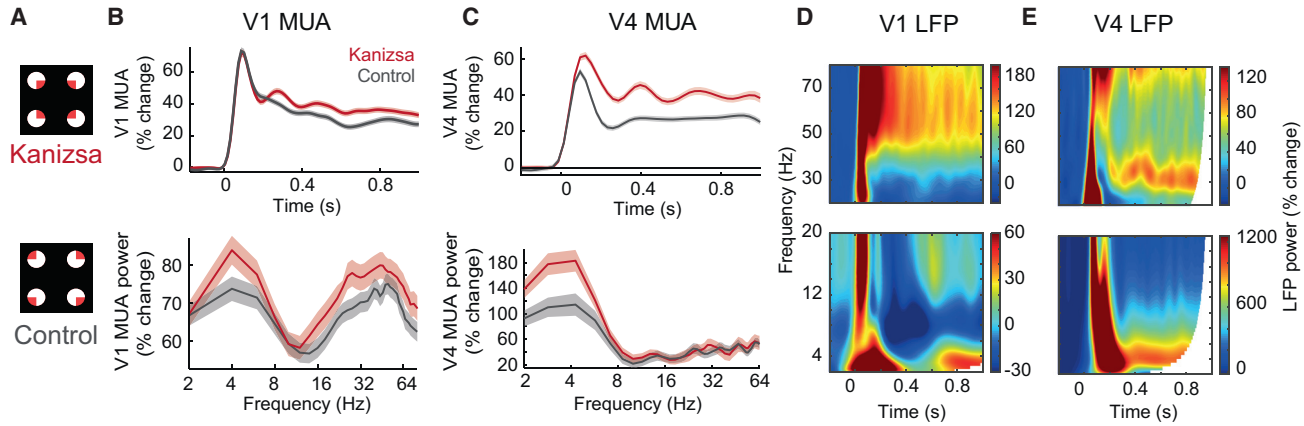

Figure 1. Rhythmic Theta Activity in V1 and V4 in Response to the Kanizsa Illusion

(A) Depiction of the Kanizsa illusion (upper panel) and the control stimulus (lower panel).

(B) Upper panel: Example V1 MUA response from one representative electrode channel; lower panel: MUA power spectrum for area V1 averaged across channels from monkey K. Kanizsa (red) and control conditions (gray) are shown; shaded areas depict SEM.

(C) Same as (B) but for V4 (monkey B).

(D) Time-frequency representations of V1 LFP, averaged across channels from monkey K for the Kanizsa condition for low (lower panel) and high frequencies (top panel). Low and high frequencies are displayed separately due to the large increase in the theta range.

(E) Same as (D) but V4 (monkey B).

See also Figure S1 and Tables S1–S3.

also showed significant power increases in the gamma range (Figures 1E, S1C, and S1D; Table S3; see also Figure 4G, left and right panel, left wings). Both the theta and gamma activity in V4 proved sensitive to the illusion (see also Figure 4H, left and right panel, left wings). As spiking and gamma oscillations can sometimes be linked to each other,[11,12] we correlated MUA and LFP gamma power and found close to zero correlations between MUA and LFP gamma power across trials in both monkeys (average r = 0.01, n = 60 in monkey B and average r = 0.02, n = 57 in monkey F). No channel showed significant correlations after correcting for multiple comparisons.

In addition to their mere presence in both areas, LFP theta and gamma oscillations showed interactions in time (Figure 2A). Such phase-to-amplitude coupling (PAC) has been proposed as a link between large-scale and local neuronal computation[13] and has been shown to *decrease* with attention-related modulation in electrocorticogram (ECoG) recordings of V1 and V4.[7] To examine this PAC further in our data, we computed a modulation index (MI)[14] in V1 and V4 (STAR Methods). We found that both V1 and V4 showed significant phase-to-amplitude coupling in the majority of channels, whereas illusion-related modulation was stronger in V4 (Figures 2B and 2C; see Table S4 for detailed statistics).

Taken together, visual stimulation elicited theta- and gamma-rhythmic MUA in V1 and theta-rhythmic MUA in V4, all of which carried information about stimulus identity. In the LFP, theta and

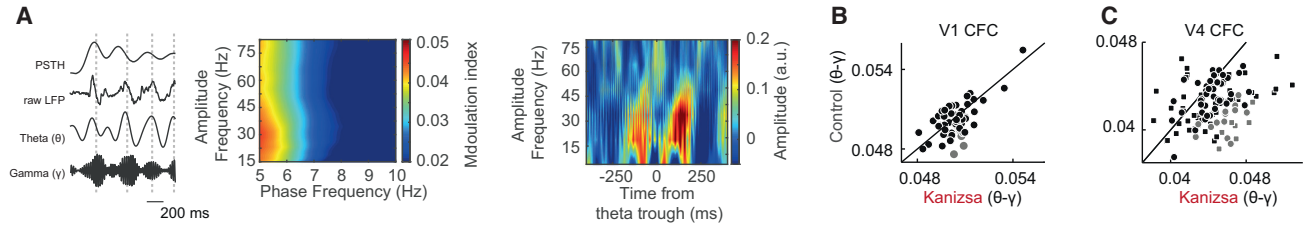

Figure 2. Theta-Phase-to-Gamma-Amplitude Coupling in V1 and V4

(A) Left panel, from top: MUA response of one example electrode channel (averaged across trials), raw LFP, as well as theta and gamma band-pass-filtered extracellular voltages for the ~−0.1–1 s trial period (monkey B, Kanizsa condition). Vertical dashed lines highlight the temporal relationship between highest gamma amplitudes to both theta LFP and theta-modulated MUA. Axes are rescaled for display purposes. Middle panel: comodulgram for modulation indices (MI) averaged across V4 channels from monkey B for the Kanizsa illusion. Right panel: theta-phase triggered spectrum from one example channel from monkey B is shown.

(B) Scatterplot showing the distribution of MI as a measure for phase-to-amplitude coupling for significantly modulated V1 electrode channels for the Kanizsa versus control conditions from monkey K. Average MI values were not significantly higher for the Kanizsa compared to the control stimulus ($p = 0.055$; n = 61; Wilcoxon paired signed rank test). Gray color highlights channels that showed significantly higher MI for the Kanizsa illusion compared to the control.

(C) Same as (B) but for V4 LFP from monkey B (circles) and F (squares) for the Kanizsa versus control conditions. Average MI values were significantly higher for the Kanizsa compared to the control stimulus ($p = 7.7 \times 10^{-9}$, n = 60 in monkey B; $p = 2.2 \times 10^{-5}$, n = 50 in monkey F; Wilcoxon paired signed rank test).

See also Table S4.

Please cite this article in press as: Kienitz et al., Theta, but Not Gamma Oscillations in Area V4 Depend on Input from Primary Visual Cortex, Current Biology (2020), https://doi.org/10.1016/j.cub.2020.10.091

CellPress
OPEN ACCESS

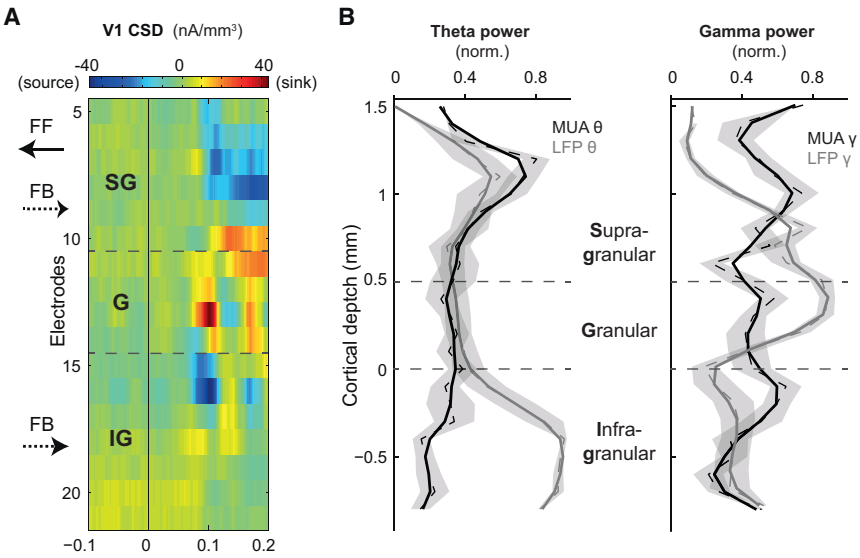

Figure 3. Laminar Distribution of Theta and Gamma Activity in V1

(A) Current source density (CSD) based on the layer-resolved LFP of a linear multi-contact electrode for one example session representing the laminar profile of visually evoked responses in V1. FB, feedback to and from V4; FF, feedforward; IG, infragranular; SG, supragranular.

(B) Left panel: average and normalized V1 MUA (black) and LFP (gray) theta power (n = 9 sessions) as a function of cortical depth. Raw data are shown as dashed, smoothed data as solid lines, and shaded areas depict SEM. Right panel: same as left panel is shown, but for V1 MUA (black) and LFP (gray) gamma power.

gamma oscillations were present both in V1 and V4. However, stimulus-specific modulation of rhythmic LFP was more prominent in V4. In addition, gamma amplitude was modulated by theta phase, with stronger illusion-specific effects in V4 and close to no illusion effects in V1.

Theta and Gamma Activity Predominantly Emerges in V1 Supragranular Layers

Having verified the presence of both theta and gamma rhythms in V1 and V4, our next aim was to assess whether their laminar cortical distribution within V1 as recorded by linear multi-contact electrodes (monkey Br; STAR Methods) is consistent with their proposed role in feedforward processing. Although feedforward projections tend to originate from supragranular layers, feedback connections preferentially target extragranular layers.[15,16] Using the laminar designation from the current source density (CSD) profile in response to visual stimulation to identify cortical layers (Figure 3A; STAR Methods),[17] we analyzed the theta-MUA as well as theta and gamma LFP as a function of V1's cortical depth (Figure 3B). This revealed that peak MUA theta power is specific to the superficial layers. For theta-range LFP, an additional peak emerged in V1's infragranular layers. Gamma-range power of the LFP peaked (supra-)granularly, in line with previous findings.[18] In summary, the predominant supragranular localization of theta and gamma oscillations supports the proposed engagement of both rhythms in feedforward processing, as V1 projections to V4 originate in supragranular layers.[15,16]

V1 Lesion Diminishes Spiking and Eliminates Theta Activity in V4

Our next aim was to experimentally test the proposed feedforward hypothesis of theta and gamma oscillations by longitudinally comparing V4 activity before and after a focal V1 lesion that causes persistent cortical blindness[19,20] and removes the major feedforward sensory input source to V4. Stimulus-specific changes were assessed by a sensitivity measure d', where positive values indicate stronger responses to the illusionary stimulus compared to the control (STAR Methods). We first examined non-rhythmic components of the recorded signals. Although lesioning V1 removed the largest part of V4 activity (Figure 4A), residual visually evoked MUA responses were still significantly present in almost all electrodes ($p < 0.05$; Wilcoxon signed rank test; Figure 4E, left panel), likely due to residual input from the V1 lesion boundary or V1-bypassing geniculate input to V4.[19,21–23] Analysis of MUA onset latencies after the lesion showed a slight delay relative to pre-lesion conditions of 13.0 ± 2 ms in monkey B ($p = 1.9 \times 10^{-10}$; n = 59) and 7.7 ± 0.5 ms in monkey F ($p = 3.8 \times 10^{-4}$; n = 54). However, the stimulus selectivity related to the visual illusion was greatly diminished in monkey B or even lost in monkey F after the lesion (d' of Kanizsa-modulated channels; p(pre > post): $p = 1 \times 10^{-6}$, n = 37 in monkey B; $p = 2 \times 10^{-5}$, n = 24 in monkey F; Wilcoxon signed rank test; Figure 4F, left panel). The stimulus selectivity related to the visual illusion was thus virtually lost after the V1 lesion. We then used spectral analysis to assess the rhythmic nature of the recorded signals. We first describe the results for theta and in the following section for gamma, as the results differed dramatically for these two rhythms.

Following the V1 lesion, V4 theta rhythmicity disappeared both for MUA and LFP (see Figures 4B, 4C, and S2A; see Table S5 for further statistics). This loss of theta activity was seen throughout our sampled population. The average theta power for the MUA channels that were visually responsive in the theta range dropped from an average of 167% ± 21% in monkey B and 79% ± 16% in monkey F to the non-significant noise level with residual values of 24% ± 12% and 33% ± 9% in monkeys B and F, respectively (Figure 4E, right panel; Table S5). Not surprisingly, the corresponding Kanizsa MUA theta d' values dropped from 0.37 ± 0.03 and 0.27 ± 0.02 to non-significant values close to zero in monkey B and F, respectively (Figure 4F, right panel; Table S5).

Analysis of LFP theta oscillations paralleled observations in the MUA domain. The prominent peak in the theta range and its modulation by the illusion stimulus given intact V1 (Figures 1E and 4C) virtually disappeared after the lesion (Figures 4C, 4G, and 4H, left panel; Table S5; signal-to-noise ratio (SNR) > 0: p = 0.46, n = 60 in monkey B; p = 0.99, n = 50 in monkey F; Wilcoxon signed rank test). Similarly, LFP-derived theta d' values (Figure 4H, left panel) were no longer significantly positive once V1 was removed (p = 0.28, n = 59 in monkey B; p = 0.99, n =

Please cite this article in press as: Kienitz et al., Theta, but Not Gamma Oscillations in Area V4 Depend on Input from Primary Visual Cortex, Current Biology (2020), https://doi.org/10.1016/j.cub.2020.10.091

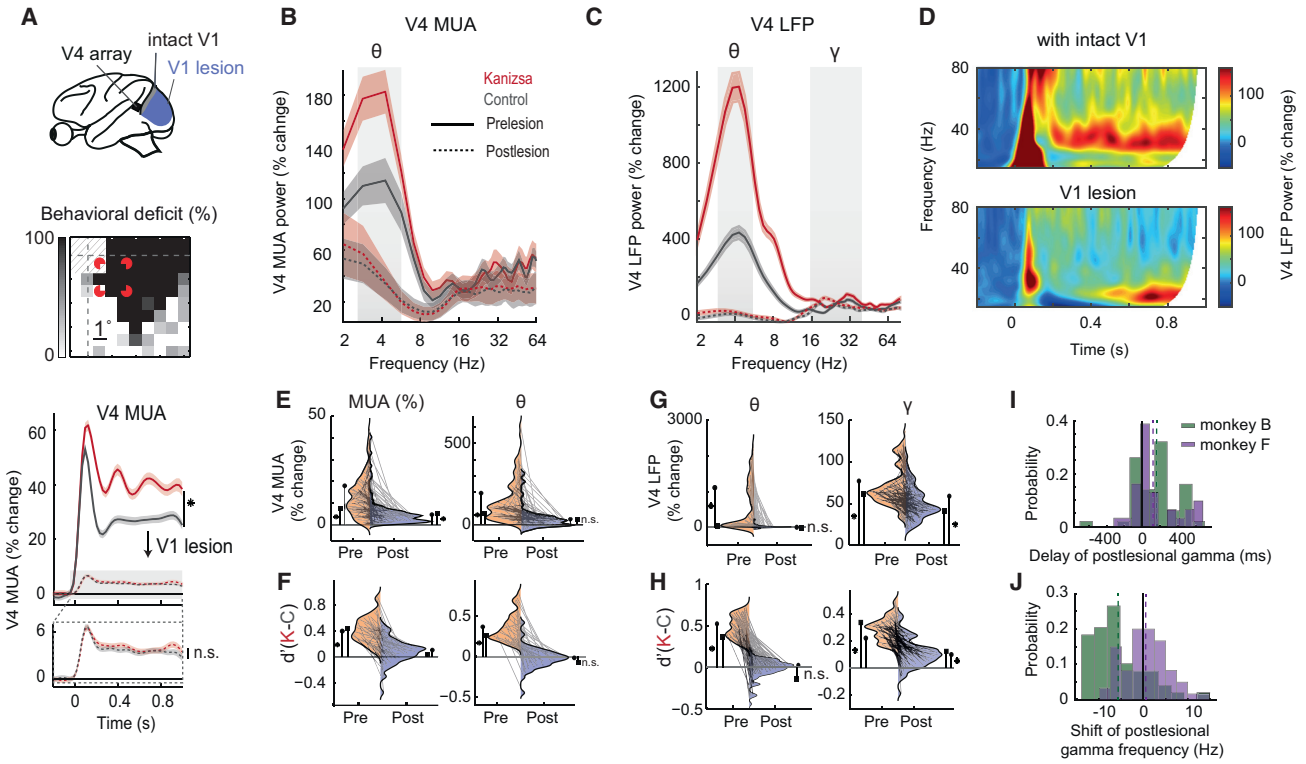

Figure 4. Effect of V1 Lesion on Rhythmic Neuronal Activity in V4

(A) Diagram indicating the extent of the focal V1 aspiration lesion (top panel). Middle panel shows the visual deficit of monkey B in a spatial detection task following the lesion (lower right quadrant); note that this scotoma covered the Kanizsa stimulus (in red for display purpose) approximately by half. Lower panel depicts V4 MUA response from one example electrode channel from monkey B before (solid lines) and after the focal V1 lesion (dashed lines) for the Kanizsa illusion (red) and control condition (gray). Post-lesional activity is shown (rescaled) in lower magnified panel. Shaded areas depict SEM.

(B) MUA power spectrum averaged across channels from monkey B for Kanizsa illusion (red) and control condition (gray) pre- (solid lines) and post-lesion (dashed lines), showing the elimination of theta activity. Shaded areas depict SEM.

(C) Same as (B) but LFP power spectrum averaged across channels from monkey B. Note the preservation of activity in the gamma range despite the elimination of theta oscillations.

(D) Time-frequency representations of one example V4 electrode channel form monkey B, depicting high LFP frequencies before (upper panel) and after the focal V1 lesion (lower panel).

(E) Distributions of MUA (left panel) and theta modulation of MUA (right panel) before (orange, left wings) and after the V1 lesion (blue, right wings) for the Kanizsa illusion. Individual pairs represent individual channels (data averaged across trials) and are shown for monkey B and monkey F; lateral symbols depict means (circle for monkey B; square for monkey F). Asterisks denote significance relative to zero (n.s., non-significant) and refer to consistent results for both monkeys.

(F) Same as (E) but for d' values (Kanizsa illusion versus control) based on MUA (left panel) and theta modulation of MUA (right panel).

(G) Distributions of LFP theta (left panel) and gamma power changes (right panel) before (orange, left wings) and after the V1 lesion (blue, right wings) for the Kanizsa illusion. Individual connected data pairs represent individual channels (data averaged across trials) and are shown for monkey B and monkey F; lateral symbols depict means (circle for monkey B; square for monkey F). Asterisks denote significance relative to zero and refer to consistent results for both monkeys.

(H) Same as (G) but for d' values (Kanizsa illusion versus control) based on LFP theta (left) and gamma power (right). Note that, although theta activity lost its Kanizsa association, gamma responses maintained information about the Kanizsa stimulus even without V1.

(I) Histogram showing the distribution of the post-lesional gamma delay across LFP channels for monkeys B (green) and F (purple). Positive values indicate a later onset of gamma power after the V1 lesion. Vertical dashed lines highlight mean values for both monkeys.

(J) Histogram showing the distribution of post-lesional shift in peak gamma frequency across LFP channels for monkeys B (green) and F (purple). Positive values indicate an increase of the peak gamma frequency after the V1 lesion. Vertical dashed lines highlight mean values for both monkeys.

See also Figure S2 and Table S5.

27 in monkey F; Wilcoxon signed rank test). Thus, although non-rhythmic residual visual activation was present in both monkeys, the neural theta rhythm and its illusion-related modulation completely vanished when V1 input was removed.

V4 Gamma Oscillations Survive V1 Lesion

The observed dependence of V4 theta rhythms on V1 input did not hold for LFP gamma, for which lesioning V1 appeared to have little effect. In fact, visually elicited activity in the low gamma band remained clearly present, despite the severed V1 input (Figures 4C, 4D, and S2B). V4 LFP gamma power responses, averaged across trial time (Figure 4G, right panel), decreased after the V1 lesion (−16.0% ± 5.13%, n = 60, in monkey B and −31.9% ± 2.22%, n = 57 in monkey F) but remained overall positive (SNR > 0: $p = 3.9 \times 10^{-11}$, n = 60 in monkey B; p = 0.001, n = 57 in monkey F; Wilcoxon signed rank test). Even more surprisingly, gamma power was still significantly modulated by the Kanizsa illusion compared to its control condition (d' > 0: $p = 7.4 \times 10^{-7}$, n = 36

Please cite this article in press as: Kienitz et al., Theta, but Not Gamma Oscillations in Area V4 Depend on Input from Primary Visual Cortex, Current Biology (2020), https://doi.org/10.1016/j.cub.2020.10.091

in monkey B and $p = 1.9 \times 10^{-7}$, n = 47 in monkey F; Wilcoxon signed rank test; Figure 4H, right panel). We performed again a correlation between post-lesion LFP gamma power and residual MUA across trials per channel and found only very weak correlation in both monkeys (r = 0.04, n = 60 in monkey B and r = 0.02, n = 57 in monkey F). Only 5 channels in monkey B and 0 channels in monkey F showed significant correlations across trials (Student's t test, corrected for multiple comparisons). Thus, in our data, there seemed to be very little relation between V4 MUA and LFP gamma oscillations. This pattern was present under intact conditions and did not change when V1 was lesioned.

Interestingly, however, the onset of gamma activity in V4 post-lesion increased by >100 ms compared to pre-lesion conditions (Figures 4D and S2B). On average, following the V1 lesion, gamma power responses significantly exceeded pre-stimulus baseline levels 161.12 ± 31.04 ms and 121.01 ± 43.69 ms after they did so with intact V1 in monkey B ($p = 5.2 \times 10^{-6}$; n = 50; Wilcoxon signed rank test) and F (p = 0.0058; n = 31; Wilcoxon signed rank test), respectively (Figure 4I; see Figure S2C for absolute latencies). This marked delay by >100 ms in gamma oscillation onset is in contrast with the finding for MUA, for which the onset latency increased by <15 ms post-lesion. Further analysis of the gamma onset latency as function of recording sessions after the V1 lesion showed that significant gamma power was present in each recording session and that there was no consistent effect regarding changes over time across monkeys (which might have been due to post-lesional plasticity; Figure S2E).

In addition, we found a decrease in peak gamma frequency without V1 in one monkey (Figure S2B). Specifically, gamma peak frequencies changed on average by −5.73 ± 0.86 Hz in monkey B ($p = 1.29 \times 10^{-6}$; n = 49; Wilcoxon signed rank test) and 0.51 ± 0.64 Hz in monkey F (p = 0.51; n = 60; Wilcoxon signed rank test), respectively, compared to pre-lesion conditions (Figure 4J; see Figure S2D for absolute frequencies).

In summary, although residual MUA responses could still be visually elicited in V4 following V1 lesions, theta activity and Kanizsa-associated modulations of spiking activity were lost. In contrast, gamma activity was well preserved and even contained stimulus-related information that emerged with a significant time delay compared to pre-lesion conditions.

DISCUSSION

Theta Rhythms across the Cortical Hierarchy

In primates, spiking and LFP theta oscillations have been observed in various cortical as well as subcortical structures during a variety of cognitive tasks.[24–35] Our results show that theta oscillations are present in the spiking of neurons both in V4 and V1. However, whether theta emerges across these cortical areas (like V1 and V4) in parallel via independent local processes[2] or whether it is coordinated to enhance long-range interareal communication[32,36,37] remains to be solved. In our data, theta organized gamma oscillations[38] and might be a candidate mechanism for long-distance integration or transfer of information to high-level association areas.[32,39,40]

The predominant supragranular occurrence of MUA theta in V1 is in line with it being a feedforward signal,[15,16,41] given that supragranular layers project to downstream visual areas. In addition, we found an infragranular peak of LFP theta oscillations. This finding might reflect the LFP's sensitivity to synaptic signals,[42,43] in principle arising from either local or remote sources,[15,16,41] and therefore does not contradict the feedforward hypothesis of theta. The infragranular LFP theta peak could point toward an integrative role of theta oscillations: although the supragranular MUA theta arguably reflects oscillatory spiking of feedforward projection units, infragranular LFP theta oscillations could reflect local postsynaptic oscillations that might serve to integrate incoming feedback signals to the local computations (e.g., via PAC to gamma oscillations) or to the theta-rhythmic feedforward output. In that sense, theta might also help to integrate feedback signals.

In a direct test of the hypothesis that theta spiking represents a feedforward signal[6] by lesioning V1 and recording from V4, our data provide first causal evidence that this may indeed be the case. A theta rhythm that emerges first in early visual cortex and is then transmitted into higher cognitive and motor areas appears as an attractive mechanism for long-range coordination of local activity. This could help explain the widespread observations of theta oscillations across a wide set of visuo-motor tasks in various areas, including attentive sampling, saccadic exploration, and motor tracking.[3,26,27,44–46] A loss of theta oscillations and stimulus-related information in spiking, as seen here under conditions of cortical blindness from V1 injury, might be indicative of a disrupted cortical information transfer and neurological dysfunction.

Unlikely Role of Gamma as Feedforward Signal

Perhaps the most surprising finding of our study is that, compared to theta oscillations, gamma oscillations in V4 remained less affected by the lesion in V1, which is at odds with the proposal of gamma as a feedforward signal.[6,10,47] What might then be the source of this V1-independent gamma in V4? One possibility is that it may reflect weak preserved gamma-rhythmic V1 input from the border of the lesion zone. Although we cannot entirely rule out this scenario, it seems unlikely, as it would involve an intact V1–V4 transmission circuit that cannot easily explain the >100 ms delayed emergence of the gamma response with little change in amplitude. A similar interpretation of post-lesional gamma activity as a mere reflection of (non-rhythmic) residual MUA appears also unlikely: for one, under our testing conditions, there was no significant correlation between MUA and LFP gamma power before as well as after the V1 lesion. Whereas the lesion delayed MUA onset in V4 by <15 ms relative to pre-lesion conditions, LFP gamma power was delayed by >100 ms after the lesion. Though it is tempting to compare residual V1 input to low-contrast stimulation conditions, the latency delay accounted for stimulation at low contrast[48–50] would only explain the delay in MUA, but not the more pronounced effect in the LFP. A third possibility, that this gamma oscillation is a result of microsaccades,[51] also appears unlikely, given the narrowband frequency range of the oscillation and its sustained time course. A fourth possibility builds up on the thalamic, V1-bypassing inputs to V4, which can account for at least part of the residual activity in V4. Yet that gamma in V4 is inherited from direct input from the lateral geniculate nucleus (LGN) or pulvinar appears unlikely, again due to latency considerations and also as gamma has so far not been reported for these brain structures. Irrespective of the actual source of the input source to V4 in our experiments,

these inputs are able to induce sufficiently strong interactions between local excitatory and inhibitory networks within V4 to generate gamma. Our results thus hint at a very local origin of gamma oscillations within the microcircuit of an area. According to this view, a visual stimulus will drive a sweep of excitation across cortical areas that is associated with subsequent increases in gamma response in each area, simply due to the repeated gamma-generating microarchitecture in each area. However, secondary synchronization of local excitatory activity might be a very useful marker of ongoing interareal communication.

In this study, we tested the hypothesis that theta and gamma rhythms act as sensory feedforward signals from V1 to V4 when monkeys viewed a visual contour illusion. With intact cortex, both oscillations were present in both areas, interacted in time, and showed stronger illusory contour-related activity in V4. Although their predominant occurrence in V1 supragranular layers is consistent with a feedforward circuit, a direct causal test revealed a clear difference for the two rhythms: although lesioning V1 eliminated the theta rhythm of V4, gamma rhythms were less affected. This result supports the proposed function for feedforward processing from V1 to V4 of theta, but not gamma rhythms and poses, together with the increasing literature body of the stimulus dependency of gamma,[52–55] limits on the proposed role of gamma as a feedforward mechanism.

STAR★METHODS

Detailed methods are provided in the online version of this paper and include the following:

- KEY RESOURCES TABLE
- RESOURCE AVAILABILITY
  - Lead Contact
  - Materials Availability
  - Data and Code Availability
- EXPERIMENTAL MODEL AND SUBJECT DETAILS
- METHOD DETAILS
  - Behavioral task and visual stimulation
  - Neurophysiology and chronic cortical lesioning
- QUANTIFICATION AND STATISTICAL ANALYSIS
  - Data preprocessing
  - Spectral analysis
  - Cross-frequency coupling
  - Analysis of laminar V1 data
  - Statistics

SUPPLEMENTAL INFORMATION

Supplemental Information can be found online at https://doi.org/10.1016/j.cub.2020.10.091.

ACKNOWLEDGMENTS

This work was supported by an intramural NIH research grant to D.A.L. (ZIA-MH002838); a National Eye Institute training grant (2T32 EY007135-21) to K.D.; an Alfred P. Sloan Fellowship, a research grant by the Whitehall Foundation, and a career starter grant by the Knights Templar Eye Foundation to A.M.; a research grant from the National Eye Institute (1R01EY027402-02) to A.M. and M.C.S.; and Emmy Noether grant 2806/1 and ERC grant OptoVision 637638 to M.C.S.

AUTHOR CONTRIBUTIONS

Conceptualization, A.M., D.A.L., and M.C.S.; Methodology, A.M., D.A.L., R.C.S., and M.C.S.; Software, A.M., D.A.L., M.A.C., K.D., R.K., J.T.S., and M.C.S.; Formal Analysis, R.K.; Investigation, A.M., D.A.L., R.C.S., R.K., M.A.C., K.D., and M.C.S.; Writing – Original Draft, R.K. and M.C.S.; Writing – Review & Editing, all authors; Supervision, M.C.S.; Funding Acquisition, A.M., D.A.L., and M.C.S.

DECLARATION OF INTERESTS

The authors declare no competing interests.

Received: July 19, 2020
Revised: October 8, 2020
Accepted: October 29, 2020
Published: December 4, 2020

REFERENCES

1. Womelsdorf, T., Fries, P., Mitra, P.P., and Desimone, R. (2006). Gamma-band synchronization in visual cortex predicts speed of change detection. Nature *439*, 733–736.
2. Kienitz, R., Schmiedt, J.T., Shapcott, K.A., Kouroupaki, K., Saunders, R.C., and Schmid, M.C. (2018). Theta rhythmic neuronal activity and reaction times arising from cortical receptive field interactions during distributed attention. Curr. Biol. *28*, 2377–2387.e5.
3. Fiebelkorn, I.C., Saalmann, Y.B., and Kastner, S. (2013). Rhythmic sampling within and between objects despite sustained attention at a cued location. Curr. Biol. *23*, 2553–2558.
4. Landau, A.N., and Fries, P. (2012). Attention samples stimuli rhythmically. Curr. Biol. *22*, 1000–1004.
5. Dugué, L., Marque, P., and VanRullen, R. (2015). Theta oscillations modulate attentional search performance periodically. J. Cogn. Neurosci. *27*, 945–958.
6. Bastos, A.M., Vezoli, J., Bosman, C.A., Schoffelen, J.-M., Oostenveld, R., Dowdall, J.R., De Weerd, P., Kennedy, H., and Fries, P. (2015). Visual areas exert feedforward and feedback influences through distinct frequency channels. Neuron *85*, 390–401.
7. Spyropoulos, G., Bosman, C.A., and Fries, P. (2018). A theta rhythm in macaque visual cortex and its attentional modulation. Proc. Natl. Acad. Sci. USA *115*, E5614–E5623.
8. Bosman, C.A., Schoffelen, J.-M., Brunet, N., Oostenveld, R., Bastos, A.M., Womelsdorf, T., Rubehn, B., Stieglitz, T., De Weerd, P., and Fries, P. (2012). Attentional stimulus selection through selective synchronization between monkey visual areas. Neuron *75*, 875–888.
9. Grothe, I., Neitzel, S.D., Mandon, S., and Kreiter, A.K. (2012). Switching neuronal inputs by differential modulations of gamma-band phase-coherence. J. Neurosci. *32*, 16172–16180.
10. van Kerkoerle, T., Self, M.W., Dagnino, B., Gariel-Mathis, M.-A., Poort, J., van der Togt, C., and Roelfsema, P.R. (2014). Alpha and gamma oscillations characterize feedback and feedforward processing in monkey visual cortex. Proc. Natl. Acad. Sci. USA *111*, 14332–14341.
11. Burns, S.P., Xing, D., and Shapley, R.M. (2010). Comparisons of the dynamics of local field potential and multiunit activity signals in macaque visual cortex. J. Neurosci. *30*, 13739–13749.
12. Nir, Y., Fisch, L., Mukamel, R., Gelbard-Sagiv, H., Arieli, A., Fried, I., and Malach, R. (2007). Coupling between neuronal firing rate, gamma LFP, and BOLD fMRI is related to interneuronal correlations. Curr. Biol. *17*, 1275–1285.
13. Canolty, R.T., and Knight, R.T. (2010). The functional role of cross-frequency coupling. Trends Cogn. Sci. *14*, 506–515.
14. Aru, J., Aru, J., Priesemann, V., Wibral, M., Lana, L., Pipa, G., Singer, W., and Vicente, R. (2015). Untangling cross-frequency coupling in neuroscience. Curr. Opin. Neurobiol. *31*, 51–61.

15. Felleman, D.J., and Van Essen, D.C. (1991). Distributed hierarchical processing in the primate cerebral cortex. Cereb. Cortex *1*, 1–47.

16. Markov, N.T., Vezoli, J., Chameau, P., Falchier, A., Quilodran, R., Huissoud, C., Lamy, C., Misery, P., Giroud, P., Ullman, S., et al. (2014). Anatomy of hierarchy: feedforward and feedback pathways in macaque visual cortex. J. Comp. Neurol. *522*, 225–259.

17. Maier, A., Aura, C.J., and Leopold, D.A. (2011). Infragranular sources of sustained local field potential responses in macaque primary visual cortex. J. Neurosci. *31*, 1971–1980.

18. Maier, A., Adams, G.K., Aura, C., and Leopold, D.A. (2010). Distinct superficial and deep laminar domains of activity in the visual cortex during rest and stimulation. Front. Syst. Neurosci. *4*, 1–11.

19. Schmid, M.C., Schmiedt, J.T., Peters, A.J., Saunders, R.C., Maier, A., and Leopold, D.A. (2013). Motion-sensitive responses in visual area V4 in the absence of primary visual cortex. J. Neurosci. *33*, 18740–18745.

20. Schmiedt, J.T., Maier, A., Fries, P., Saunders, R.C., Leopold, D.A., and Schmid, M.C. (2014). Beta oscillation dynamics in extrastriate cortex after removal of primary visual cortex. J. Neurosci. *34*, 11857–11864.

21. Rodman, H.R., Sorenson, K.M., Shim, A.J., and Hexter, D.P. (2001). Calbindin immunoreactivity in the geniculo-extrastriate system of the macaque: implications for heterogeneity in the koniocellular pathway and recovery from cortical damage. J. Comp. Neurol. *431*, 168–181.

22. Fries, W. (1981). The projection from the lateral geniculate nucleus to the prestriate cortex of the macaque monkey. Proc. R. Soc. B: Biol. Sci. *213*, 73–80.

23. Schmid, M.C., Mrowka, S.W., Turchi, J., Saunders, R.C., Wilke, M., Peters, A.J., Ye, F.Q., and Leopold, D.A. (2010). Blindsight depends on the lateral geniculate nucleus. Nature *466*, 373–377.

24. Fuster, J.M., and Alexander, G.E. (1973). Firing changes in cells of the nucleus medialis dorsalis associated with delayed response behavior. Brain Res. *61*, 79–91.

25. Ramcharan, E.J., Gnadt, J.W., and Sherman, S.M. (2005). Higher-order thalamic relays burst more than first-order relays. Proc. Natl. Acad. Sci. USA *102*, 12236–12241.

26. Hall, T.M., de Carvalho, F., and Jackson, A. (2014). A common structure underlies low-frequency cortical dynamics in movement, sleep, and sedation. Neuron *83*, 1185–1199.

27. Susilaradeya, D., Xu, W., Hall, T.M., Galán, F., Alter, K., and Jackson, A. (2019). Extrinsic and intrinsic dynamics in movement intermittency. eLife *8*, e40145.

28. Jutras, M.J., Fries, P., and Buffalo, E.A. (2013). Oscillatory activity in the monkey hippocampus during visual exploration and memory formation. Proc. Natl. Acad. Sci. USA *110*, 13144–13149.

29. Lakatos, P., Shah, A.S., Knuth, K.H., Ulbert, I., Karmos, G., and Schroeder, C.E. (2005). An oscillatory hierarchy controlling neuronal excitability and stimulus processing in the auditory cortex. J. Neurophysiol. *94*, 1904–1911.

30. Wilke, M., Logothetis, N.K., and Leopold, D.A. (2006). Local field potential reflects perceptual suppression in monkey visual cortex. Proc. Natl. Acad. Sci. USA *103*, 17507–17512.

31. Lee, H., Simpson, G.V., Logothetis, N.K., and Rainer, G. (2005). Phase locking of single neuron activity to theta oscillations during working memory in monkey extrastriate visual cortex. Neuron *45*, 147–156.

32. Liebe, S., Hoerzer, G.M., Logothetis, N.K., and Rainer, G. (2012). Theta coupling between V4 and prefrontal cortex predicts visual short-term memory performance. Nat. Neurosci. *15*, 456–462, S1–S2.

33. Sheinberg, D.L., and Logothetis, N.K. (1997). The role of temporal cortical areas in perceptual organization. Proc. Natl. Acad. Sci. USA *94*, 3408–3413.

34. Rollenhagen, J.E., and Olson, C.R. (2005). Low-frequency oscillations arising from competitive interactions between visual stimuli in macaque inferotemporal cortex. J. Neurophysiol. *94*, 3368–3387.

35. Raghavachari, S., Kahana, M.J., Rizzuto, D.S., Caplan, J.B., Kirschen, M.P., Bourgeois, B., Madsen, J.R., and Lisman, J.E. (2001). Gating of human theta oscillations by a working memory task. J. Neurosci. *21*, 3175–3183.

36. Siapas, A.G., Lubenov, E.V., and Wilson, M.A. (2005). Prefrontal phase locking to hippocampal theta oscillations. Neuron *46*, 141–151.

37. Schmid, M.C., and Maier, A. (2015). To see or not to see–thalamo-cortical networks during blindsight and perceptual suppression. Prog. Neurobiol. *126*, 36–48.

38. Lisman, J.E., and Jensen, O. (2013). The θ-γ neural code. Neuron *77*, 1002–1016.

39. Buzsáki, G., and Wang, X.-J. (2012). Mechanisms of gamma oscillations. Annu. Rev. Neurosci. *35*, 203–225.

40. von Stein, A., Chiang, C., and König, P. (2000). Top-down processing mediated by interareal synchronization. Proc. Natl. Acad. Sci. USA *97*, 14748–14753.

41. Rockland, K.S., and Pandya, D.N. (1979). Laminar origins and terminations of cortical connections of the occipital lobe in the rhesus monkey. Brain Res. *179*, 3–20.

42. Rauch, A., Rainer, G., and Logothetis, N.K. (2008). The effect of a serotonin-induced dissociation between spiking and perisynaptic activity on BOLD functional MRI. Proc. Natl. Acad. Sci. USA *105*, 6759–6764.

43. Kajikawa, Y., and Schroeder, C.E. (2011). How local is the local field potential? Neuron *72*, 847–858.

44. Otero-Millan, J., Troncoso, X.G., Macknik, S.L., Serrano-Pedraza, I., and Martinez-Conde, S. (2008). Saccades and microsaccades during visual fixation, exploration, and search: foundations for a common saccadic generator. J. Vis. *8*, 21.1–21.18.

45. Chota, S., Luo, C., Crouzet, S.M., Boyer, L., Kienitz, R., Schmid, M.C., and VanRullen, R. (2018). Rhythmic fluctuations of saccadic reaction time arising from visual competition. Sci. Rep. *8*, 15889.

46. Landau, A.N., Schreyer, H.M., van Pelt, S., and Fries, P. (2015). Distributed attention is implemented through theta-rhythmic gamma modulation. Curr. Biol. *25*, 2332–2337.

47. Self, M.W., van Kerkoerle, T., Supèr, H., and Roelfsema, P.R. (2013). Distinct roles of the cortical layers of area V1 in figure-ground segregation. Curr. Biol. *23*, 2121–2129.

48. Reich, D.S., Mechler, F., and Victor, J.D. (2001). Temporal coding of contrast in primary visual cortex: when, what, and why. J. Neurophysiol. *85*, 1039–1050.

49. Gawne, T.J. (2000). The simultaneous coding of orientation and contrast in the responses of V1 complex cells. Exp. Brain Res. *133*, 293–302.

50. Sundberg, K.A., Mitchell, J.F., Gawne, T.J., and Reynolds, J.H. (2012). Attention influences single unit and local field potential response latencies in visual cortical area V4. J. Neurosci. *32*, 16040–16050.

51. Yuval-Greenberg, S., Tomer, O., Keren, A.S., Nelken, I., and Deouell, L.Y. (2008). Transient induced gamma-band response in EEG as a manifestation of miniature saccades. Neuron *58*, 429–441.

52. Bartoli, E., Bosking, W., Chen, Y., Li, Y., Sheth, S.A., Beauchamp, M.S., Yoshor, D., and Foster, B.L. (2019). Functionally distinct gamma range activity revealed by stimulus tuning in human visual cortex. Curr. Biol. *29*, 3345–3358.e7.

53. Gray, C.M., and Singer, W. (1989). Stimulus-specific neuronal oscillations in orientation columns of cat visual cortex. Proc. Natl. Acad. Sci. USA *86*, 1698–1702.

54. Gieselmann, M.A., and Thiele, A. (2008). Comparison of spatial integration and surround suppression characteristics in spiking activity and the local field potential in macaque V1. Eur. J. Neurosci. *28*, 447–459.

55. Peter, A., Uran, C., Klon-Lipok, J., Roese, R., van Stijn, S., Barnes, W., Dowdall, J.R., Singer, W., Fries, P., and Vinck, M. (2019). Surface color and predictability determine contextual modulation of V1 firing and gamma oscillations. eLife *8*, 1–38.

56. Oostenveld, R., Fries, P., Maris, E., and Schoffelen, J.-M. (2011). FieldTrip: Open source software for advanced analysis of MEG, EEG, and invasive electrophysiological data. Comput. Intell. Neurosci. *2011*, 156869.

57. Cox, M.A., Schmid, M.C., Peters, A.J., Saunders, R.C., Leopold, D.A., and Maier, A. (2013). Receptive field focus of visual area V4 neurons determines responses to illusory surfaces. Proc. Natl. Acad. Sci. USA *110*, 17095–17100.

58. Mitzdorf, U. (1985). Current source-density method and application in cat cerebral cortex: investigation of evoked potentials and EEG phenomena. Physiol. Rev. *65*, 37–100.

Please cite this article in press as: Kienitz et al., Theta, but Not Gamma Oscillations in Area V4 Depend on Input from Primary Visual Cortex, Current Biology (2020), https://doi.org/10.1016/j.cub.2020.10.091

STAR★METHODS

KEY RESOURCES TABLE

REAGENT or RESOURCE	SOURCE	IDENTIFIER
Deposited Data		
Data underlying the figures		https://doi.gin.g-node.org/10.12751/g-node.nb4nnp
Experimental Models: Organisms/Strains		
Macaca mulatta	Public Health England, Porton Down, UK	Monkey K
Macaca mulatta	Wake Forest University (Winston-Salem, North Carolina)	Monkey Br
Macaca mulatta	NIH Primate Services, Poolesville, USA	Monkey B Monkey F
Software and Algorithms		
MATLAB	The MathWorks	https://www.mathworks.com/products/matlab.html
Fieldtrip toolbox	[56]	https://www.fieldtriptoolbox.org/
Other		
Infrared video eye tracking system	EyeLink	https://www.sr-research.com
Data Acquisition System	Blackrock Microsystems	https://blackrockmicro.com
Data Acquisition System	Tucker Davis Technology system	https://www.tdt.com
Data Acquisition System	Plexon, UProbe	https://plexon.com

RESOURCE AVAILABILITY

Lead Contact

Further information and requests for resources should be directed to and will be fulfilled by the Lead Contact, Ricardo Kienitz (ricardo.kienitz@esi-frankfurt.de).

Materials Availability

This study did not generate new unique items, such as animal lines or reagents.

Data and Code Availability

The data underlying the figures were deposited on a public repository (https://doi.gin.g-node.org/10.12751/g-node.nb4nnp).

EXPERIMENTAL MODEL AND SUBJECT DETAILS

Two healthy adult female and two male rhesus monkeys (*Macaca mulatta*, monkey B, F, K and Br) were used in the study (Table S6). All procedures were in accordance with the Institute for Laboratory Animal Research Guide for the Care and Use of Laboratory Animals and approved by the Animal Care and Use Committees of the National Institute of Mental Health and Vanderbilt University or by the Regierungspräsidium Darmstadt in accordance with EU directive 2010/63. All surgeries were carried out aseptically under general anesthesia using standard techniques including peri-surgical analgesia and monitoring. Each monkey received a head-immobilization implant and an implant to record neural data (see section below on Neurophysiology). Throughout the study animal welfare was monitored by veterinarians, technicians and scientists.

METHOD DETAILS

Parts of the dataset underlying this study (V4 data from monkey B and F) have been analyzed and published with regard to the dependence of a Kanizsa-specific increase in single (and multi-) unit spiking on the receptive field focus[57]. The respective study did not study oscillatory signals.

Please cite this article in press as: Kienitz et al., Theta, but Not Gamma Oscillations in Area V4 Depend on Input from Primary Visual Cortex, Current Biology (2020), https://doi.org/10.1016/j.cub.2020.10.091

Behavioral task and visual stimulation

Each monkey was trained to maintain fixation within a 1-1.5° diameter window centered on a small red spot (0.2° diameter, white for monkey K) during the presentation of various visual stimuli. To map receptive fields, white random dot kinematograms (1.5° diameter, see[57] for details) were shown on a black background at 64 different positions in the lower right visual hemifield. The Kanizsa illusion and the control stimulus consisted of four inducers (~1° diameter) located at (1°, −1°), (3°, −1°), (1°, −3°) and (3°, −3°), presented for 1 s (1.5 s in V1 recordings) after 1 s of fixation baseline. Each inducer consisted of a white disk with one quarter of the circle colored in red, giving them a "pacman-like" appearance. For the illusory stimulus, the red quarter faced the inner illusory surface (IF1 in[57]) creating an illusory rectangle. The control stimulus consisted of inducers that were rotated by 180° such that the red cutouts were facing outward (CF1 in[57]). For monkey K, the stimulus position was adapted to the V1 receptive fields (center of stimulus: x = 1°, y = −4.2°). V1 receptive field centers ranged from 0.06° to 4.7° and from −6.7° to −0.9° along the horizontal and vertical meridian respectively. For the laminar V1 recordings, the Kanizsa stimulus and its control were positioned such that the receptive field focus (RFF, see[57]) of the recording site was centered on the illusory parts of the stimulus.

Neurophysiology and chronic cortical lesioning

Neurophysiological data was recorded via chronically implanted multi-microelectrode ("Utah") arrays that were located in area V4 (monkeys B and F) or V1 (monkey K) (see[19] for details regarding surgery and implantation). Each electrode was spaced 400 μm from its neighboring electrodes, and 1.5 mm (0.6 and 1.5 mm for monkey K) long. Neural data from monkeys B and F was recorded at a sampling rate of 24414.1 Hz using a Tucker Davis Technology system and at 30 kHz for monkeys K and Br on a Blackrock Microsystems Cerebus System. Following 13 sessions in monkey B and 6 sessions in monkey F, permanent focal aspiration lesions of isohemispheric primary visual cortex (V1) were performed (see[23] for details). After the lesion, post-lesion data were recorded in 15 and 6 sessions for monkey B and monkey F, respectively. To confirm the visual deficit (scotoma) following the V1 lesion, monkeys performed a perimetry task covering the lower right quadrant (see[20] for details). Data from monkey K was collected in two sessions. Layer-resolved V1 data was recorded from monkey Br using a linear microelectrode array, consisting of 22-24 active microelectrodes, linearly spaced 0.1 mm apart, with impedances ranging 0.2-0.8 MΩ at 1kHz (UProbe, Plexon). Electrical reference for data from the UProbe was the probe shaft.

QUANTIFICATION AND STATISTICAL ANALYSIS

Data preprocessing

All neurophysiological data were processed and analyzed using custom-written code for MATLAB (MathWorks, Inc.) and the FieldTrip MATLAB toolbox[56]. The continuous recordings were separated into individual stimulus presentations (trials) using digital event markers aligned on stimulus onset. We focused our analyses on the sustained response period 300-1000 ms after stimulus onset, excluding the transient onset response. Trials containing motion artifacts were excluded by visual inspection without knowledge of trial type. Four dysfunctional recording channels in monkey B, four in monkey F and two in monkey K were excluded from the analysis. Details on receptive field mapping can be found in Cox et al.[57] An estimate for multi-unit activity (MUA) was obtained from the high frequency envelope: MUA was extracted by high-pass filtering (300-12000 Hz), followed by rectification, and low-pass filtering (120 Hz) of the broadband data (see[19] for further details). The local field potential (LFP) was obtained by low-pass filtering the signal at 256 Hz. Data from microelectrode arrays was pooled across sessions. In order to assess the stimulus-specific effects of the Kanizsa illusion, data were normalized using the average baseline value (−0.7 – 0 s of prestimulus fixation period). MUA and powerspectra are expressed as percent change from this baseline.

Spectral analysis

To obtain the spectral profile of MUA and LFP responses, we used a Hanning-tapered Fourier transformation. Visual inspection of the spectra revealed peaks in the 3-6 Hz and 25-70 Hz bands (monkey B: 25-40, monkey F: 30-60 Hz, monkey K: 40-70 Hz), which are referred to as theta and (low) gamma, respectively. To obtain time-frequency representations (Figure 1), we performed a wavelet transform based on Morlets. To optimally assess low and high frequency components, we separately analyzed frequencies from 1-20 Hz ("low frequencies," width 3 cycles, 1.3 Hz bandwidth at 4 Hz, 0.01 Hz steps) and > 20 Hz ("high frequencies," width 7 cycles, 15.7 Hz bandwidth at 40 Hz). As described above, analyses including spectral assessment focused on the sustained response period 300-1000 ms after stimulus onset.

Cross-frequency coupling

In order to assess phase-to-amplitude coupling between theta and gamma oscillations in the LFP, we computed a modulation index *MI* as follows[14]: The original LFP Signal $S(t)$ was bandpass-filtered into the theta and gamma ranges, respectively, using a two-pass filter (fourth order Butterworth) to avoid frequency-dependent phase shifts: $S_\theta(t)$ and $S_\gamma(t)$. As a next step, the Hilbert transform h of both signals was computed, producing complex values whose real components represent the amplitude of the signal and the imaginary part represent phase: $h(S_\theta(t))$ and $h(S_\gamma(t))$. From the Hilbert-transformed signals we extracted the phases of the theta signal $\Phi_{S_\theta}(t)$ and the amplitude from the gamma signal $A_{S_\gamma}(t)$. The composite signal $[\Phi_{S_\theta}(t),\ A_{S_\gamma}(t)]$ describes the amplitude of S_γ at each phase of S_θ. The phases $\Phi_{S_\theta}(t)$ were then binned ($n = 18$) and the mean amplitude $\langle A_{S_\gamma}\rangle(j)$ over each bin j was calculated and normalized by dividing by the sum of all bins, resulting in the normalized distribution-like function $P(j)$. Finally, the Modulation Index (MI) was defined as the normalized Kullback-Leibler divergence (KL) computed between $P(j)$ and a uniform distribution $Q(j)$ as follows:

Please cite this article in press as: Kienitz et al., Theta, but Not Gamma Oscillations in Area V4 Depend on Input from Primary Visual Cortex, Current Biology (2020), https://doi.org/10.1016/j.cub.2020.10.091

$$D_{KL}(P,\ Q) = \sum_{j=1}^{n} P(j) loglog\left(\frac{P(j)}{Q(j)}\right)$$

$$MI = \frac{D_{KL}}{log(n)}$$

We tested for significant modulation using a Monte Carlo technique, where we randomly permuted the amplitude-signal trial-wise against the phase-signal 500 times. To test for significant differences between Kanizsa illusion and control conditions, we performed a matched non-parametric test (Wilcoxon signed rank test) across channels. *MI* comes with several caveats (see[14] for a discussion). To avoid an overestimation of phase-amplitude coupling we verified that (1) there were clear peaks in the TFR and powerspectrum at the frequencies of interest (theta and gamma) and (2) that frequency band used for amplitude (gamma, 25-50 Hz) was at least double the frequency we used for the phase signal (theta, 3-6 Hz). To compute the Comodulogram (Figure 2A, middle panel) phase frequencies ranged from 5 to 10 Hz (±2 Hz) and amplitude frequencies from 15 to 80 Hz (±10 Hz). To compute the theta-phase triggered spectrogram (Figure 2A, right panel), the amplitude of bandpass-filtered high frequency (ranging from 10 to 80 Hz) was triggered on theta oscillation troughs and averaged across trials.

Analysis of laminar V1 data

To obtain a more localized measure of neural activity based on the LFP, and to locate electrodes on the U-Probe across cortical layers, we computed the laminar current source density (CSD) by approximating the second spatial derivative of the LFP[58]. The CSD constitutes a measure of localized current flow, which can be used to delineate upper from middle and lower cortical layers[17]. The transition from granular to infragranular layers was visually identified by selecting the bottom of the initial response sink of the CSD profile of the respective recording session[17]. We computed the laminar theta power based on MUA[43] and the laminar theta and gamma power based on LFP. The average laminar profiles were smoothed by fitting a spline for display purpose. Significance was assessed using a one-sided Wilcoxon signed rank test against baseline, n = 9).

Statistics

All statistical tests were done in MATLAB (MathWorks, Inc.) using their standard-implementation or custom-written code. Average values of the measures defined above (spectral power, PPC, MI) were calculated as the mean value across time and frequency. Differences between conditions were tested with nonparametric Wilcoxon signed rank tests (paired data) or to test if a distribution was significantly greater/smaller than zero, Mann-Whitney U tests (equals Wilcoxon rank sum test, unpaired data) or the computational resampling statistics described above. Data was smoothed for display purposes. To quantify effect sizes associated with the illusory stimulus, we computed the sensitivity measure

$$d' = \frac{\mu_K - \mu_C}{\sqrt{\frac{1}{2}\left(\sigma_K^2 + \sigma_C^2\right)}},$$

where μ_K and μ_C are the sample means and σ_K and σ_C the standard deviations for the Kanizsa and control conditions, respectively. To assess the strength of any residual theta rhythm (post lesion) we computed the signal-to-noise ratio:

$$SNR = 20\ \frac{\varphi_\theta}{\varphi_n},$$

where φ_θ and φ_n are the power values in the theta (signal) and high frequency (noise) ranges (15-25 Hz (MUA) and 128-256 (LFP)), respectively. The percentage of variance explained was assessed by computing how well one signal predicted the other using a multilinear regression model. For the latency analysis (Figure 4I) we assessed the post-stimulus time point (excluding the initial transient, i.e., t > = 0.2 s) where gamma power significantly exceeded baseline levels on a channel-by-channel basis. Significance in this context was assessed using the Wilcoxon rank sum test for each post-stimulus time point across trials, followed by a Bonferroni-Holm correction. The time-point of reaching significance equaled the time-point where p values within a sliding moving average window of 100 ms fell below alpha = 0.05 for the first time. Time points were then compared before and after the V1 lesion.

For the peak shift analysis (Figure 4J) pre- and post-lesional gamma peaks were defined as the strongest peak (as detected by the 'findpeaks' MATLAB function) in the gamma range after subtracting a fitted polynomial of degree 1 from the spectra (which allowed for better detection of smaller peaks) on a channel-by-channel basis. Gamma peaks were then compared before and after the V1 lesion.

Current Biology, Volume *31*

Supplemental Information

Theta, but Not Gamma Oscillations in Area V4 Depend on Input from Primary Visual Cortex

Ricardo Kienitz, Michele A. Cox, Kacie Dougherty, Richard C. Saunders, Joscha T. Schmiedt, David A. Leopold, Alexander Maier, and Michael C. Schmid

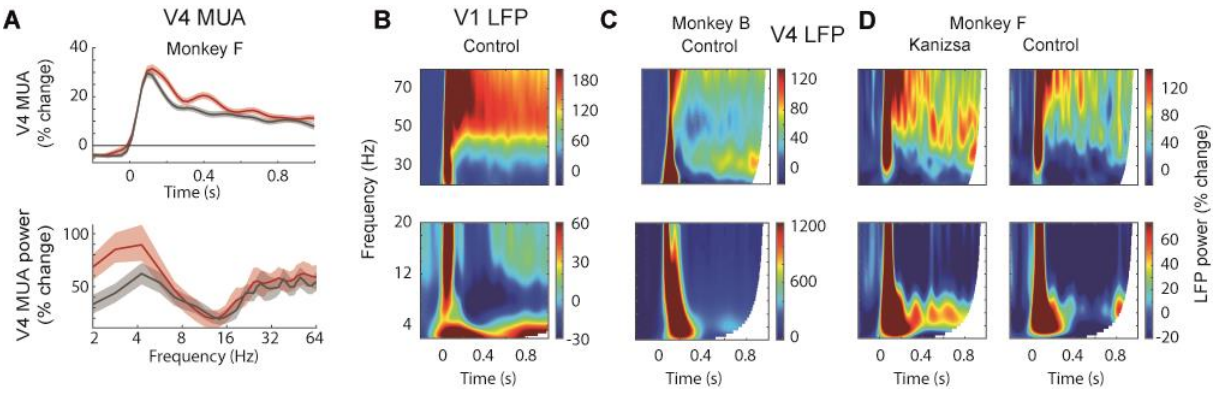

Figure S1. Theta and gamma oscillations in V1 and V4. Related to Figure 1.

(A) Same as Figure 1C, but for monkey F. Upper panel: example V4 MUA response from one representative electrode channel; lower panel: MUA powerspectrum for area V4 averaged across channels from monkey F. Kanizsa (red) and control conditions (gray), shaded areas depict SEM.

(B) Same as Figure 1D, but for the control condition. Time-frequency representations of V1 LFP, averaged across channels from monkey K for the control condition for low (lower panel) and high frequencies (top panel).

(C) Same as Figure 1E, but for the control condition. Time-frequency representations of V4 LFP, averaged across channels from monkey B for the control condition for low (lower panel) and high frequencies (top panel).

(D) Time-frequency representations of V4 LFP, averaged across channels from monkey F for the Kanizsa (left panels) and control condition (right panels) for low (lower panel) and high frequencies (top panel).

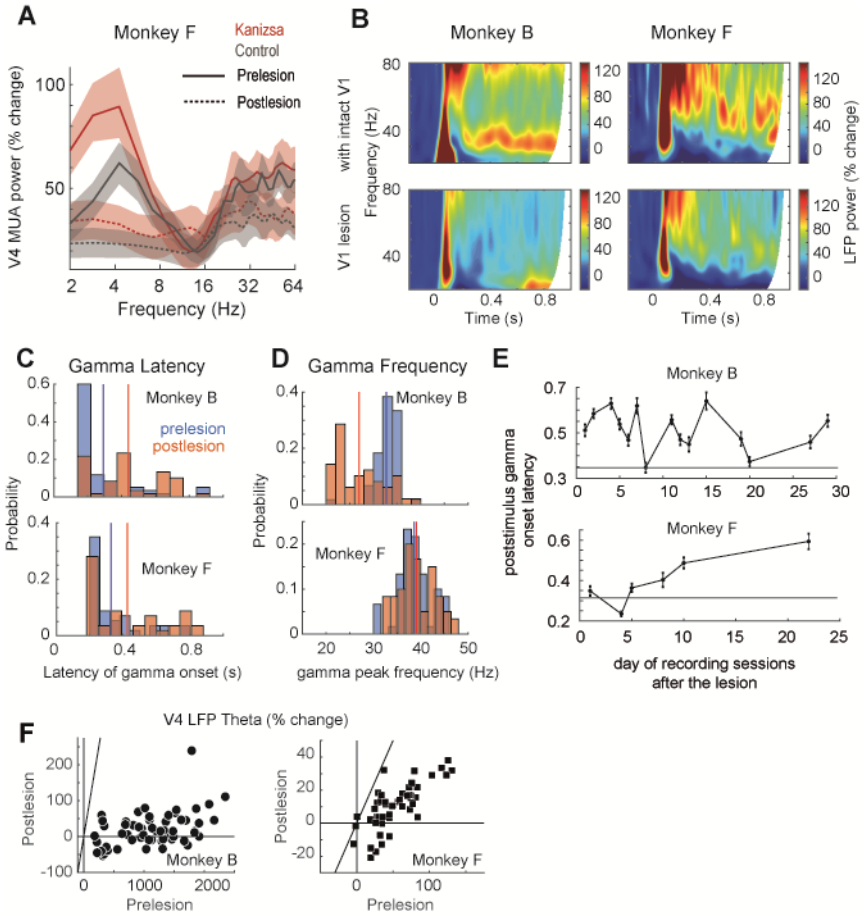

Figure S2. V4 theta and gamma oscillations after V1 lesion. Related to Figure 4.

(A) Same as Figure 4B, but for monkey F. MUA powerspectrum averaged across channels from monkey F for Kanizsa illusion (red) and control condition (gray) pre- (solid lines) and postlesion (dashed lines), showing the elimination of theta activity. Shaded areas depict SEM

(B) Time-frequency representations of V4 LFP, averaged across channels from monkey B (left panels) and monkey F (right panels) before (upper panels) and after the V1 lesion (lower panels). Note the presevation and delayed onset of gamma ocillations after the lesion.

(C) Histograms showing the distribution of the gamma onset latencies after stimulus onset across LFP channels for monkey B (upper panel) and monkey F (lower panel) before (blue) and after the lesion (orange). Vertical lines highlight mean values.

(D) Same as **(C)** but for gamma peak frequencies.

(E) Poststimulus gamma onset latencies as a function of postlesional recording sessions (e.g. day 1 = first recording session of the described experiments after the V1 lesion, not the first day after the lesion) averaged across LFP channels for monkey B (upper panel) and monkey F (lower panel). Horizontal lines depict prelesional mean latencies. Errorbars depict SEM.

(F) Same as Figure 4 G, left panel, but presenting data from both monkeys separately as scatter plots depicting V4 LFP theta power change distributions pre vs. postlesion for monkey B (left panel) and F (right panel). Each dot/square represents data from a single channel, averaged across trials.

Table S1. MUA statistics with intact V1. Related to Figure 1.

Area	MUA increase for Kanizsa condition (mean ± SEM)	MUA increase for control condition (mean ± SEM)	Statistics (illusion > control, Wilcoxon paired signed rank test)	Related Figures
V1 (monkey K)	10.1±1.29%	9.4±1.36%	p=0.07, n=61	Figure 1B
V4 (monkey B)	18.1±1.15%	14.9±1.17%	p=6.6x10^{-6}, n=59	Figure 1C (upper panel), Figure 4E-F, left panels and wings)
V4 (monkey F)	7.7±0.76%	6.9±0.77%	p=0.001, n=54	Figure S1A (upper panel), Figure 4E-F, left panels and wings)

Table S2. V1 and V4 MUA oscillation statistics with intact V1. Related to Figure 1.

Area	Theta power increase for Kanizsa condition (mean ± SEM)	Theta power increase for control condition (mean ± SEM)	Number of channels with significant theta increase to visual stimulation ($p < 0.05$, Wilcoxon signed rank test)	Statistics (illusion> control, Wilcoxon paired signed rank test)	Gamma Power increase for Kanizsa condition (mean ± SEM)	Gamma Power increase for control condition (mean ± SEM)	Number of channels with significant theta increase to visual stimulation ($p < 0.05$, Wilcoxon signed rank)	Statistics (illusion> control, Wilcoxon paired signed rank test)	Related Figures
V1 (monkey K)	81.5 ± 2.89%	72.3±3.12%	61/61 (100%)	p=0.01, n=61	78.2±2.36%	72.6±2.39%	61/61 (100%)	p=0.03, n=61	Figure 1B
V4 (monkey B)	167.3±21.29%	128.7±28.39%	59/59 (100%)	p=1.1x10^{-5}, n=59	-	-	-	-	Figure 1C
V4 (monkey F)	79.4±16.45%	63.3±10.34%	31/54 (57%)	p=0.18, n=31	-	-	-	-	Figure S1A

Table S3. V1 and V4 LFP oscillation statistics with intact V1. Related to Figure 1.

Area	Number of channels with significant power increase to visual stimulation ($p < 0.05$, Wilcoxon signed rank test)	Number of channels with significant illusion-specific power increase ($p<0.05$, Wilcoxon rank sum test)	Statistics (illusion>control, Wilcoxon paired signed rank test)	Related Figures
Theta				
V1 (monkey K)	61/61 (100%)	3/61 (4.9%)	p=0.99, n=61	Figure 1D, S1B
V4 (monkey B)	60/60 (100%)	59/60 (98%)	p=8.4x10^{-12}, n=60	Figure 1E, S1C
V4 (monkey F)	50/60 (83%)	27/50 (54%)	p=5.9x10^{-10}, n=50	Figure S1D
Gamma				
V1 (monkey K)	61/61 (100%)	10/61 (16.4%)	p=0.97, n=61	Figure 1D, S1B
V4 (monkey B)	60/60 (100%)	36/60 (60%)	p=8.4x10^{-12}, n=60	Figure 1E, S1C
V4 (monkey F)	57/60 (95%)	47/57 (82%)	p=2.6x10^{-11}, n=57	Figure S1D

Table S4. PAC statistics with intact V1. Related to Figure 2.

Area	MI for Kanizsa condition (mean ± SEM)	MI for control condition (mean ± SEM)	Statistics (illusion>control, Wilcoxon paired signed rank test)	Number of channels with significant PAC (p<0.05, permutation test)	Number of significantly illusion-modulated channels (p<0.05, Wilcoxon rank sum test)	Mean theta phase of highest gamma amplitude (mean ± SEM, illusion condition, 0° being the theta peak)	Related Figures
V1 (monkey K)	0.050±0.0001	0.050±0.0002	p=0.055, n=61	61/61 (100%)	4/61 (6.5%)	151±6.7°	Figure 2B
V4 (monkey B)	0.045±0.0003	0.042±0.0002	p=7.7x10^{-9}, n=60	60/60 (100%)	13/60 (21.6%)	-37±2.2°	Figure 2C
V4 (monkey F)	0.044±0.0005	0.042±0.0003	p=2.2x10^{-5}, n=50	50/60 (83%)	7/50 (14%)	29±8.2°	Figure 2C

Table S5. Postlesion MUA and LFP oscillation statistics. Related to Figure 4.

Monkey	Statistics power (Pre>Post, Wilcoxon paired signed rank test)	Statistics postlesion (SNR>0, Wilcoxon signed rank test)	d' prelesion (mean ± SEM)	d' postlesion (mean ± SEM)	Statistics d' (Pre>Post, Wilcoxon paired signed rank test)	Statistics d' postlesion (d'>0, Wilcoxon signed rank test)	Related Figures
MUA – Theta							
Monkey B	p=1.4x10^{-6}, n=59	p=0.75, n=59	0.37±0.03	-0.01±0.02	p=8.5x10^{-9}, n=42	p=0.79, n=42	Figure 4E-F, right panels
Monkey F	p=5.2x10^{-4}, n=31	p=0.91, n=31	0.27±0.02	-0.07±0.10	p=0.01, n=7	p=0.89, n=7	Figure 4E-F, right panels
LFP –Theta							
Monkey B	p=8.3x10^{-12}, n=60	p=0.46, n=60	0.53±0.02	0.03±0.01	p=1.2x10$^{-11,}$ n=59	p=0.28, n=59	Figure 4G-H, left panels
Monkey F	p=4.4x10^{-10}, n=50	p=0.99, n=50	0.37±0.01	-0.14±0.03	p=2.9x10^{-06}, n=27	p=0.99, n=27	Figure 4G-H, left panels
LFP – Gamma							
Monkey B	p=7.6x10^{-6}, n=60	p=3.9x10^{-11}, n=60	0.22±0.01	0.10±0.01	p=3.3x10^{-7}, n=36	p=7.4x10^{-7}, n=36	Figure 4G-H, right panels
Monkey F	p=3.8x10^{-11}, n=57	p=0.001, n=57	0.34±0.01	0.12±0.02	p=3.2x10^{-9}, n=47	p=1.9x10^{-7}, n=47	Figure 4G-H, right panels

Table S6. Recordings performed in individual monkeys. Related to STAR Methods.

Recordings / Monkey	Monkey B	Monkey F	Monkey K	Monkey Br
V4 Utah-Array before and after V1 lesion	X	X		
V1 Utah-Array			X	
V1 linear U-Probe				X